Sensors and Materials, Vol. 37, No. 12 (2025) 5343–5355
MYU Tokyo

S & M 4248

Detection of Zinc Ions Using a Fluorescent Compound Derived from a Cyanoacrylic Acid-based Chemosensor

Prawonwan Thanakit,[1] Supakorn Puengvigrai,[1] Teeranuch Khummung,[1]
Songwut Suramitr,[2] Koson Trachu,[1] and Darinee Phromyothin[1*]

[1]Department of Nanoscience and Nanotechnology, School of Integrated Innovative Technology,
King Mongkut's Institute of Technology Ladkrabang, Bangkok 10520, Thailand
[2]Department of Chemistry, Faculty of Science, Kasetsart University,
Bangkok 10900, Thailand

(Received June 18, 2025; accepted October 17, 2025)

Keywords: cyanoacrylic acid-based molecule, fluorescent chemosensor, Zn^{2+} ions, TD-DFT

This study was initially conducted through the synthesis and characterization of a cyanoacrylic acid based on thiophene-phenylethyl-cyanoacrylic acid (TPC). The receptor cyanoacrylic acid derivative revealed an "off-on" mode with high selectivity and sensitivity to Zn^{2+} ions, whereas the selectivity of the optical sensor for Zn^{2+} ions was the consequence of chelation-enhanced fluorescence. The possible interference of other metal ions in solution was examined in the presence of different types of metal ion, whereby the results showed high selectivity and sensitivity with a low detection limit of 7.78×10^{-8} M. Furthermore, the geometry of the TPC molecular structure and electronic properties were examined using density functional theory and time-dependent density functional theory. A comparison between calculation and experimental data yielded results indicating that the compound has potential applications in chemosensors.

1. Introduction

Zinc is the second most abundant essential metal ion found in the human body. It plays a major role in biochemical processes, including acting as a cofactor of hundreds of enzymes and a component of regulators of gene expression. It is also a critical element in human pathophysiology, neurology, and apoptosis.[1,2] Importantly, the World Health Organization has also recommended a maximum acceptable Zn^{2+} concentration in drinking water of 5.0 mg L^{-1}.[3] However, no matter how essential Zn^{2+} ions are for normal growth and development, their excessive accumulation can lead to cell death. For example, excessive amounts of Zn^{2+} ions can disrupt and reduce microbial activities, thus causing phytotoxic effects in the soil.[4–7] Therefore, accurate and sensitive Zn^{2+} ion detection is needed and of great importance for environmental, human, and ecological health.[8–11]

Research on using fluorescence probes to detect Zn^{2+} and other metal ions has attracted considerable attention.[12,13] Among various detection methods, the fluorescence sensing

*Corresponding author: e-mail: darinee.ph@kmitl.ac.th
https://doi.org/10.18494/SAM5760

ISSN 0914-4935
https://myukk.org/

technique is popular owing to its nondestructive nature, high selectivity and sensitivity, real-time response, and naked-eye detection possibility.[14,15] A fluorescence sensor must meet two basic requirements: first, the ligand molecule must produce a fluorescence signal (signal selectivity), and second, the receptor must have a strong affinity to the intended ion (binding selectivity).[16] By using a suitable organic molecule ligand, one can improve the sensor for better ion binding and increase its sensitivity.[17]

Organic molecule ligands are widely used in various applications owing to their unique optical and electronic properties. These properties make them essential in fields such as catalysis, sensors, and drug development. As researchers continue to explore their potential, the demand for innovative organic ligands is expected to grow significantly. Some of their remarkable characteristics include their easy-to-design and easy-to-synthesize structure, high purity, and high processability.[18,19] Thiophene and its polymerized derivatives are commonly used in organic electronic devices and molecular electronics owing to the presence of a sulfur atom in an aromatic molecule, which confers additional stabilization and excellent transport properties to its oligomers.[20] Furthermore, thiophene is a member of a class of heterocyclic sulfur compounds with a five-membered ring,[21] which is one of the most significant classes of heterocyclic compounds. Its structure is similar to that of pyrrole, and its conjugated π-system contributes to excellent electron delocalization, making thiophene derivatives highly fluorescent and perfect for signal transduction in chemosensors.[22] Additionally, thiophene can be attached to various heterocyclic systems, giving rise to new compounds that exhibit a broad range of biological effects and reduced toxicity.[23] Most fluorescence sensors based on conjugated organic molecules are capable of fluorescing at a higher or lower intensity when binding with a specific ion.[24,25] Sensing mechanisms also take account of photo-induced electron transfer,[26] intramolecular charge transfer,[27] metal-ligand charge transfer,[28] and twisted intramolecular charge transfer.[29]

In this study, we developed a new fluorescence sensor from a thiophene derivative [thiophene-phenylethyl-cyanoacrylic acid (TPC)]. The five-membered heteroaromatic compound thiophene was employed as conjugating units in designing a novel donor–acceptor structure. TPC is composed of thiophene, aromatic rings, and cyanoacrylic acid moieties. The cyanoacrylic acid moieties provide selective binding sites for Zn^{2+} ions over other competitive metal ions. A Job plot, a method of continuous variation, was carried out to determine the stoichiometry of ligand–metal complexes.[30] Moreover, to better understand the geometrical and electronic properties of the molecule, computational calculations based on the density functional theory (DFT) and time-dependent density functional theory (TD-DFT) together with the CAM-B3LYP/6-31G(d,p) method were performed.

2. Experimentation

2.1 Materials

3-Bromothiophene, 4-formylphenylboronic acid, tetrabutylammonium bromide (TBAB), tetrakis (triphenylphosphine) palladium, and cyanoacetic acid were purchased from Aldrich,

whereas *N*-bromosuccinimide and piperidine were purchased from Merck. All other chemicals were used as received without further purification. Deionized water was used throughout the experiment. ^{1}H NMR spectra were recorded on an INOVA VARIAN 400 MHz spectrometer. UV–vis spectroscopy was realized on a PG Instrument T90+ spectrophotometer. Fluorescence spectra were recorded using a Perkin-Elmer LS 55 spectrophotometer. The mass spectrum (MS) was obtained with a GC 6890N (Agilent Technologies, USA) and an MS 5973N (Agilent Technologies, USA). Finally, FT-IR spectra were taken using KBr disks with a Perkin Elmer Model System-2000 spectrometer.

2.2 Syntheses

2.2.1 Synthesis of thiophene-phenylaldehyde (1)

3-Bromothiophene (10 mmol, 0.1014 g) was dissolved in toluene under N_2, to which 4-formylphenylboronic acid (10 mmol, 0.0884 g), TBAB (0.6 g), and potassium carbonate (30 ml) were later added. The mixture was stirred for half an hour at RT under N_2, then tetrakis(triphenylphosphine)palladium(0) (0.1 g) was added, followed by heating to 90 °C for 24 h. The organic layer was dried over anhydrous sodium sulfate, and the solvent was removed under reduced pressure. The residue was purified by column chromatography using dichloromethane:ethyl acetate (10:1 v/v) and gave a reaction yield of 40%. The ^{1}H NMR (DMSO-d6, 400 MHz) of thiophene-phenylaldehyde(1) exhibits a chemical shift at 10.00 (s, ^{1}H, -aromatic-C=CHO), 7.90 (s, ^{1}H, - aromatic-CH=C), 7.76 (m, 4H, aromatic-CHO), 7.39 (d, 2H, aromatic-dithieno), and 7.26 (s, ^{1}H, dithieno).

2.2.2 Synthesis of thiophene-phenylethyl-cyanoacrylic

Compound (1) (0.48 mmol, 0.0417 g) and cyanoacetic acid (0.94 mmol, 0.0447 g) were combined in acetonitrile while nitrogen gas was present, and then 20 drops of piperidine were added. The mixture was heated and stirred for 20 h under nitrogen gas, and then the solvent was removed by reducing the pressure. The residue was purified by column chromatography using dichloromethane:ethyl acetate (10:1 v/v) and gave a reaction yield of 60%. The ^{1}H NMR (DMSO-d6, 400 MHz) of TPC exhibits a chemical shift at 7.90 (s, 1H, - aromatic-C<u>H</u>=C), 7.76 (m, 4H, aromatic-CHO), 7.39 (d, 2H, aromatic-dithieno), 7.26 (s, 1H, dithieno) FT-IR (KBr, cm^{-1}): ν_{max} 1,614.23 (C=C), 1,723.24 (C=O), 2,257.67 (C=N), 2,862.67 and 2,932.40 (CH), and 3,414.84 (OH). MS (GC-MS): calculated for $C_{14}H_9O_2SN$ [M]: m/z 256.

2.3 UV–vis and fluorescence titration

TPC receptors were dissolved in dimethylformamide (DMF) (2.5×10^{-5} mol L^{-1}) and used for metal ion sensing titration experiments. Stock solutions of Mn^{2+}, Fe^{2+}, Co^{2+}, Ni^{2+}, Cu^{2+}, Zn^{2+}, Cd^{2+}, Hg^{2+}, and Pb^{2+} were prepared from their acetate salts. In these titration experiments, TPC solution was added to the solution of each metal ion and diluted with DMF. All fluorescence

spectra were excited at 325 nm. Fluorescence spectra of Zn-TPC complexes were also measured in the presence of other competitive metal ions (5×10^{-5} mol L^{-1} of).

2.4 Theoretical model and calculation

Theoretical studies were performed using the density functional three-parameter, CAM-B3LYP with the LanL2DZ basis set for Zn atoms and the 6-31G(d,p) basis set for the remaining atoms of TPC without any symmetry restrictions. The solvent effects in DMF were modeled through the Polarizable Continuum Model. After the optimization of the molecule geometry, the singlet-to-singlet vertical electronic transition energies were calculated by TD-DFT using the same functional and basis set. For the fluorescence energies, the geometry optimization of the first excited singlet state was carried out with TD-DFT gradients. All the calculations were performed using the Gaussian 09 program package.[31]

3. Results and Discussion

3.1 Synthesis

For the synthesis of the TPC chemosensor, 3-bromothiophene was reacted with 4-phenylboronic acid and with a tetrakis(triphenylphosphine)palladium(0) catalyst under a basic condition in a Suzuki coupling reaction. The Suzuki coupling reaction transformed the aldehyde functional group of the thiophene-phenylaldehyde into the cyanoacrylic acid (COOH, C≡N) group by the Knoevenagel reaction with a piperidine catalyst; thereby, the TPC receptor was obtained as shown in Fig. 1.

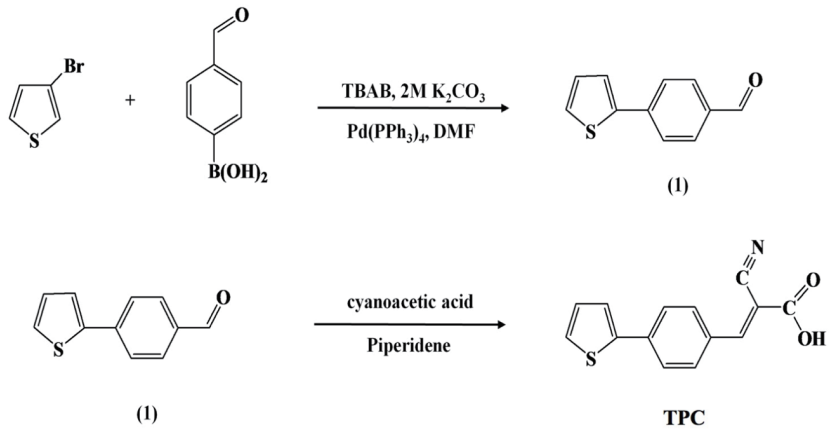

Fig. 1. Synthesis of thiophene-phenylethyl-cyanoacrylic acid chemosensor.

3.2 Optical and electronic properties of TPC

The TPC molecule was composed of thiophene, aromatic ring, and cyanoacrylic acid moieties. The electron-donating group in the thiophene moiety was conjugated to the electron-withdrawing group in the cyanoacrylic acid moiety, causing a change in the $\pi \rightarrow \pi^*$ [highest occupied molecular orbital (HOMO) to lowest unoccupied molecular orbital (LUMO)] transition and enhancing changes in the sensor's electronic configuration and optical properties – a higher number of active binding sites and a more rigid structure as well as redshifted absorption and fluorescence spectra (Fig. 2). Through the use of an aromatic ring bridge, the charge transfer of the TPC molecule involves the transfer of an electron from the excitation state of the electron-rich thiophene group to the excitation state of the electron-deficient cyanoacrylic moiety. An analysis of the absorption and fluorescence spectra was performed to investigate the fluorescence detection behavior of TPC at λ_{max} values of 325 and 395 nm, respectively, as shown in Fig. 3. The fluorescence color becomes green when excited at 325 nm. The solvent effect causes shifts of peaks in the fluorescence spectrum because the carboxylic acid moieties (COOH) can form hydrogen bonds with polar solvent molecules. The internal charge transfer mechanism of TPC is the deprotonation of the carboxylic (COOH) group. As the solvent polarity increased, a strong

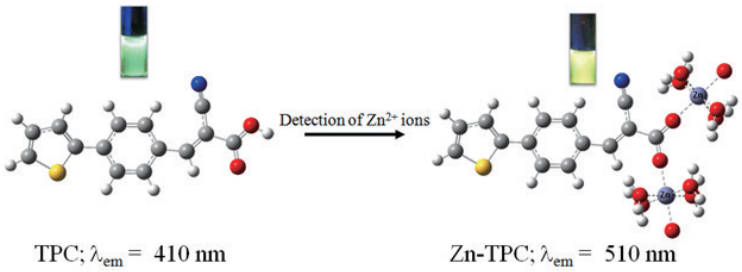

Fig. 2. (Color online) Proposed schematic structure of Zn-TPC complex in PL wavelength and intensity during Zn^{2+} addition.

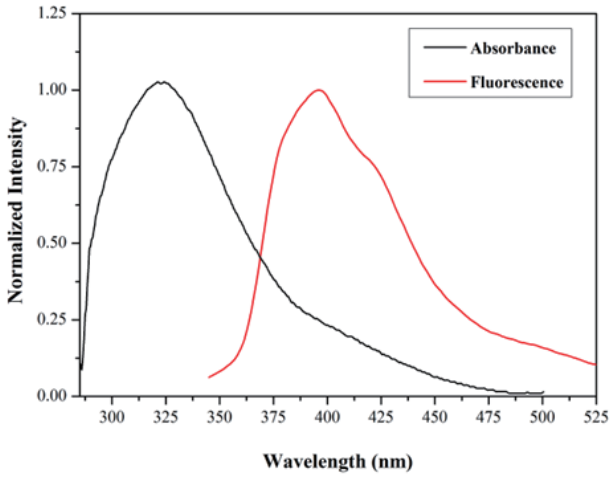

Fig. 3. (Color online) UV–vis absorption and fluorescence spectra of TPC (2.5×10^{-5} M) in DMF.

interaction between the solvent and the carboxylic acid moiety causes a redshift in emission wavelength. Therefore, DMF as the polar solvent was used in the system to increase the hydrogen bond formation with TPC because it contains a carbonyl oxygen (C=O) with a lone pair that can act as a strong hydrogen-bond acceptor. The TPC intermolecular interaction with the solvent was increased significantly by the cyano group (C≡N) because of its high polarity and ability to form a hydrogen bond.[31]

3.3 Selectivity for various metal ions

The selectivity and sensitivity of TPC to various metal ions were examined in DMF. The binding capacities of the TPC sensor (2.5×10^{-5} M) toward various metal ions (5.0×10^{-5} M) including Mn^{2+}, Fe^{2+}, Co^{2+}, Ni^{2+}, Cu^{2+}, Zn^{2+}, Hg^{2+}, and Cd^{2+} were inferred from their absorption and fluorescence spectra excited at 325 nm, as shown in Figs. 4 and 5(a), respectively. The addition of various metal ions in the TPC solution resulted in the change of the absorption spectra, that is, all metal ions caused the absorbance intensity changes but only the absorption spectra of Zn^{2+} had a broad peak, as shown in Fig. 4. The broad peaks in fluorescence spectra may indicate more complex energy distributions or electron movement patterns within the molecule, resulting in a wider emission range. Therefore, TPC and different metal ions were studied in terms of their fluorescence spectra as shown in Fig. 5(a). When Zn^{2+} or other competitive ions were added to the TPC sensor solution, its fluorescence peak at 410 nm decreased. However, only Zn^{2+} and Pb^{2+} appeared to produce a new peak at 510 nm from the extended conjugation, while the other ions did not. Moreover, Pb^{2+} only gave a much smaller peak than Zn^{2+}. As shown in Fig. 5(b), the fluorescence intensity ratio (I/I_0) at 510 nm was much higher when adding Zn^{2+} than when adding the other metal ions. This indicates that the complexation between Zn^{2+} and TPC results in the reduction in electron energy level. The

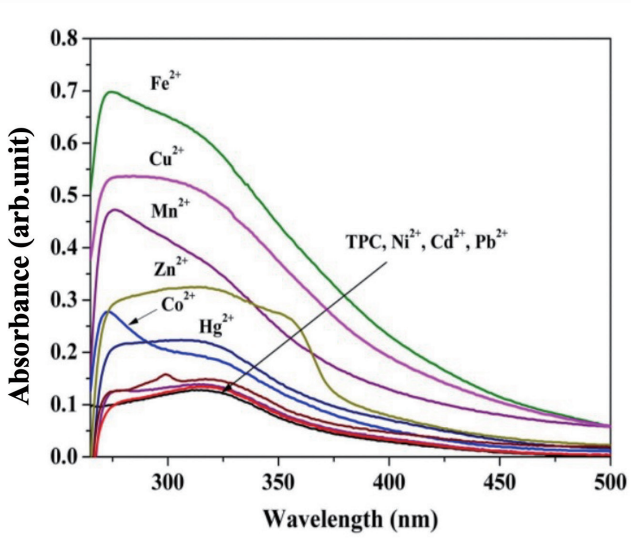

Fig. 4. (Color online) Absorption spectra of TPC (2.5×10^{-5} M) in the presence of Mn^{2+}, Fe^{2+}, Co^{2+}, Ni^{2+}, Cu^{2+}, Zn^{2+}, Cd^{2+}, Hg^{2+}, and Pb^{2+} (in DMF).

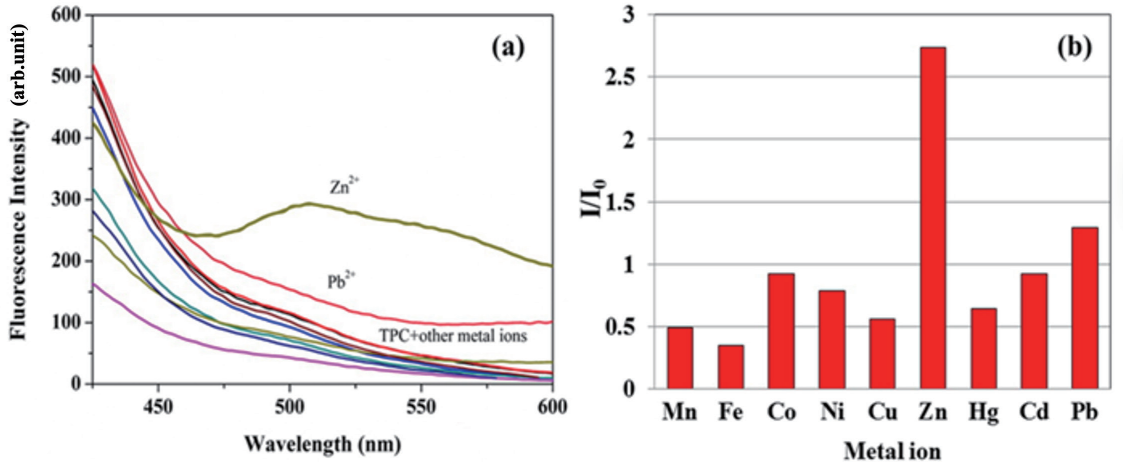

Fig. 5. (Color online) (a) Fluorescence spectra of TPC (2.5×10^{-5} M) in the presence of Mn^{2+}, Fe^{2+}, Co^{2+}, Ni^{2+}, Cu^{2+}, Zn^{2+}, Cd^{2+}, Hg^{2+}, and Pb^{2+} (in DMF). (b) Fluorescence intensity ratios (I/I_0) of these ions at 510 nm.

possible reason was that the coordination of Zn^{2+} increased the electron transfer from the donor to the acceptor in π-conjugation, causing a decrease in the HOMO-LUMO of the $\pi \rightarrow \pi^*$ interaction, which induced a redshift in the fluorescence spectrum and reduced electron transition energy.[31–33] This result indicates the high sensitivity and selectivity of TPC to Zn^{2+} because the atom binding sites of TPC preferred the Zn^{2+} coordinates better than the other metal ions. A new peak fluorescence of Zn^{2+} occurred at 510 nm, while the other metal ions did not appear as shown in Fig. 5. In addition, the TPC binding to Zn^{2+} illustrates the photo-induced charge transfer mechanism (see Sect. 3.6) occurring from the acceptor group (C≡N, COOH) binding to Zn^{2+} and then redshifted or a new wavelength.

3.4 Ratiometric sensing of Zn^{2+}

A Zn^{2+} titration experiment with TPC was carried out. It was found that increasing the Zn^{2+} concentration results in a clearly increasing fluorescence intensity as illustrated in Fig. 6(a). Increasing the Zn^{2+} concentration causes a small decrease in fluorescence intensity at 395 nm but a large increase at 510 nm. The plot of fluorescence intensity ($I–I_0$) versus Zn^{2+} concentration in Fig. 6(b) shows that the intensity was linearly proportional to the concentration in the range from 1×10^{-5} to 1×10^{-4} M with a correlation coefficient (R^2) of 0.9948. The detection limit for Zn^{2+} ions was calculated to be 77.80 ppb. Therefore, the wavelength for fluorescence detection at 510 nm was used in other subsequent experiments. Moreover, the time dependence of complex forming was investigated by determining the fluorescence intensity of complexes of TPC with Zn^{2+} ions at times between 0 and 30 min. The plots of these intensities versus time can be found in Fig. 7. The intensity responses to complex forming were immediate and remained virtually constant throughout the 30 min duration. The fluorescence intensity did not change from 0 to 30 min when Zn^{2+} was added to the TPC solution. Therefore, it did not reverse after the TPC binding to Zn^{2+}.

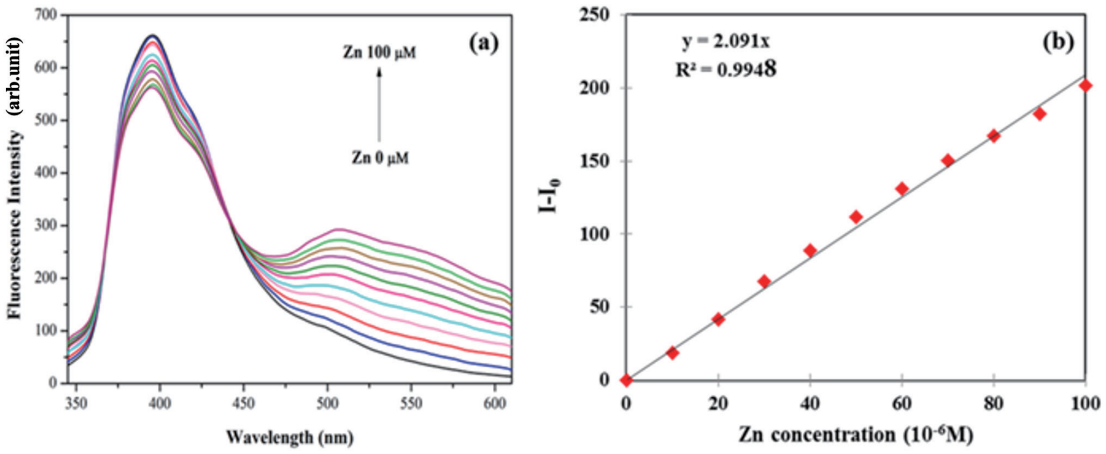

Fig. 6. (Color online) (a) Fluorescence emission spectra of TPC (2.5×10^{-5} M) in DMF at various concentrations of Zn^{2+} ions. (b) Plot of fluorescence intensity versus Zn^{2+} concentration.

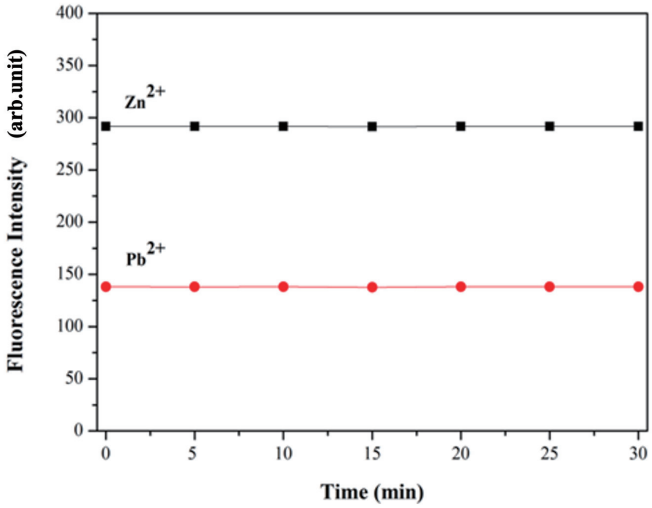

Fig. 7. (Color online) Fluorescence intensity of TPC complex with Zn^{2+} and Pb^{2+} versus time.

3.5 Selectivity toward Zn^{2+}

To determine the selectivity of Zn^{2+} ions among competitive metal ions (Mn^{2+}, Fe^{2+}, Co^{2+}, Ni^{2+}, Cu^{2+}, Zn^{2+}, Hg^{2+}, and Cd^{2+}), an interaction study was performed by adding Zn^{2+} to mixtures of TPC containing those other metal ions (5.0×10^{-5} M). Figure 8 shows the detection of TPC in the presence of various ions in combination with Zn^{2+}, compared with other free ions. When Zn^{2+} ions were added to TPC containing each metal ion, the fluorescence intensity at 510 nm remained constant or slightly decreased. The results indicate a high selectivity toward Zn^{2+} over the other ions. This indicates that the presence of Zn^{2+} significantly enhances the

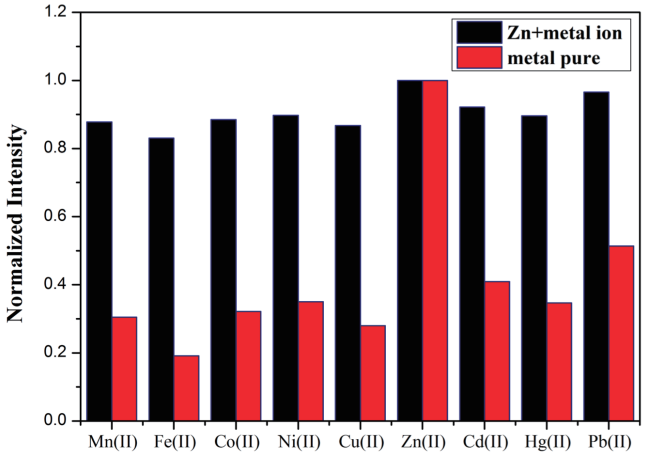

Fig. 8. (Color online) Fluorescence responses of TPC in DMF in the presence of various ions (red bar) in combination with Zn^{2+} (black bar).

fluorescence response of TPC, making it a promising candidate for applications in sensing and detection. In the next section, we explore the specific interactions between TPC and Zn^{2+} to optimize its use in various analytical methods.

3.6 Mechanism of Zn^{2+} ion sensing

A possible mechanism of TPC and Zn^{2+} binding was proposed as shown in Fig. 2. The TPC probe shows a high fluorescence intensity of Zn^{2+} at 395 nm but is not the response of TPC and Zn^{2+} complexes, which is sought at 510 nm. A Job plot at such a wavelength indicates that the stoichiometric binding between TPC and Zn^{2+} is 1:1, as illustrated in Fig. 9. The fluorescence spectra of Zn-TPC complexes indicate the changes in fluorescence wavelength and intensity depending on the metal concentration. The TPC fluorescence strengthens when an electron from a fluorophore molecule is transferred to an ionophore via internal charge transfer, resulting in fluorescence emission at 395 nm. After forming a complex with metal ions, changes in fluorescence emission occur with a shifted and new wavelength at 510 nm. This mechanism is called the photo-induced charge transfer.[34] The binding site of TPC was proposed to be its coordinating N and O atoms or O and O atoms with Zn^{2+}. It demonstrated that these atoms forming a complex with Zn^{2+} ions can alternate to electron energy levels.[35] The presence of the cyano group showed an increase in the probe's polarity and an ability to form a hydrogen bond, whereas the presence of the carboxylic groups played a crucial role in the specific recognition of Zn^{2+}.[36] These groups promoted molecular association through intermolecular hydrogen bonding and multimer formation.[37,38] The experiment also revealed that a ligand–zinc complex was formed by octahedral coordination with the ligand's N and O atoms or O and O atoms as well as two DMF molecules.[36–39] Therefore, the researchers reasoned that while the DMF molecule was bound with the ion via the O atom, the TPC ligand in this study could also be bound with Zn^{2+} via O and O (carboxylate) atoms to form a chelate ring. Generally, the C atoms of an aromatic ring act as a proton donor, whereas the O atoms of the carboxylic group and DMF

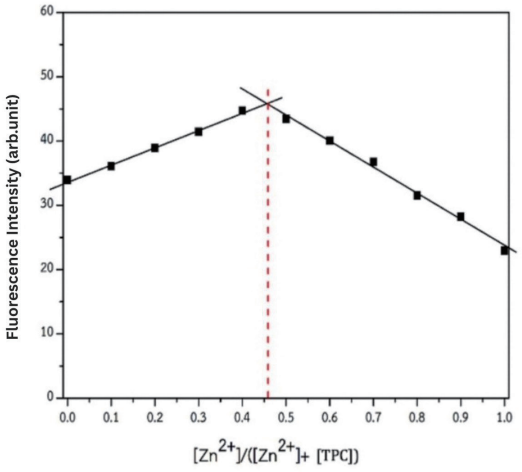

Fig. 9. (Color online) Job plot of TPC and Zn^{2+} ions.

act as a proton acceptor. From the result, it can be proposed that coordination between TPC and Zn^{2+} can increase the conformation rigidity of the complex and can make it easier for the electron from ligand to metal charge transfer that the aromatic rings transfer to Zn^{2+} ions via O and O atoms.(40)

3.7 Computational calculation

The ground state geometries of the TPC ligand and Zn-TPC complexes were optimized in the DMSO solvation by the CAM-B3LYP method. The calculated bond distances and angles are illustrated in Fig. 10. The optimized geometry of TPC shows that the HOMOs comprised π-bonding orbitals localized on the aromatic ring and cyanoacrylic moiety. On the other hand, the LUMOs consist of π*-antibonding orbitals localized on the thiophene and phenyl ring moieties. The molecular orbitals point out that the transition from the HOMO to the LUMO clearly indicates a transfer of charge from the thiophene to the cyanoacrylic moiety (C≡N, COOH). The optimized geometries of the Zn-TPC complexes show that the HOMOs and LUMOs were composed of π-bonding and π*-antibonding orbitals, respectively. The HOMO orbitals of Zn-TPC complexes were largely localized on one coordinating ligand, whereas the LUMO orbitals were mostly localized on the other coordinating ligand. However, the complexation of Zn^{2+} ions with the TPC causes a decrease in the energy of HOMO and LUMO orbitals compared with free ligands. The ΔE of the HOMO to LUMO levels of the TPC ligand (3.57 eV) is higher than that of the Zn-TPC complexes (3.64 eV). It is clear that coordination to a d10 metal center can reduce the energy gap of S0→S1 levels according to the law for radiationless deactivation.

To better understand the electronic transitions, TD-DFT calculations were performed. The vertical excitation energies, calculated at the optimized ground state geometries of the TPC ligand and Zn-TPC complexes, are in good agreement with their experimental spectra. For the TPC ligand, the lower energy S0 → S1 transitions were calculated to be 330 nm in DMF (Table 1). These transitions are mainly due to π→π* transitions within the ligand. Upon the

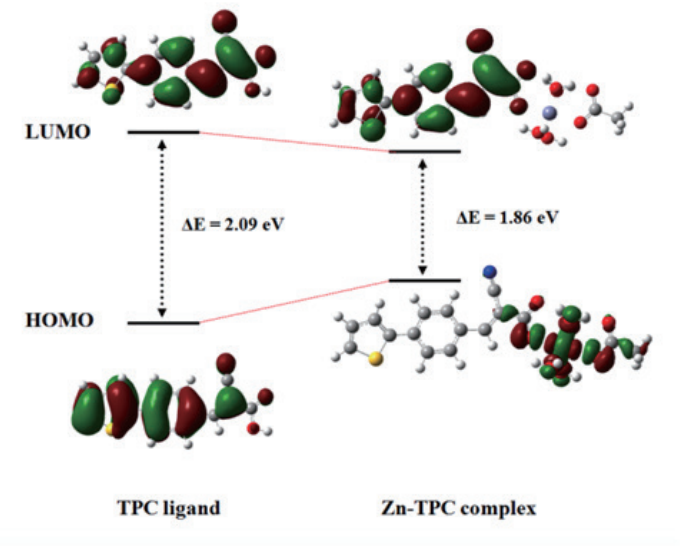

Fig. 10. (Color online) Plots of the relevant molecular orbitals from the HOMO and LUMO orbitals of TPC ligand and Zn-TPC complexes optimized from ground state geometries in the DMF solvation.

Table 1
Calculated TD-DFT excitation energies for the lowest transition, oscillator strengths (f), compositions, and their contributions.

States	Excitation transitions				
	λ (nm)	E_{gap} (eV)	f	Composition	Expt. (nm)
TPC ligand					
S0 → S1	330	3.75	1.0125	HOMO→LUMO (96%)	325
S0 → S2	270	4.59	0.0079	HOMO→L+1 (65%)	–
S0 → S3	255	4.86	0.0001	HOMO→L+2 (77%)	–
S0 → S4	247	5.03	0.0783	H-2→LUMO (30%) H-1→LUMO (30%)	–
Zn-TPC complex					
S0 → S1	340	3.65	1.2339	HOMO→LUMO (95%)	
S0 → S2	270	4.59	0.0131	HOMO→L+2 (81%)	
S0 → S3	249	4.98	0.0154	H-2→LUMO (35%)	
S0 → S4	247	5.02	0.0008	H-2→LUMO (35%)	

complexation of Zn-TPC complexes, TD-DFT calculations in DMF reveal the weak energy band in the absorption spectrum of Zn-TPC complexes to be the S0 → S1 transition (calculated at 340 nm), which could be assigned as ligand-centered π–π* transitions. The other calculated higher energy absorption bands at 340 nm with high oscillator strengths were derived from transitions from HOMOs to LUMOs. As previously shown in Fig. 8, the HOMO orbitals were mostly localized on one coordinating ligand, whereas the LUMO orbitals were localized on the other coordinating ligand. By this, the S0 → S1 transitions can be attributed to the intra-ligand π–π* transitions of the aromatic ring and cyanoacrylic moieties present in the complex.

4. Conclusions

A new fluorescence sensor molecule, TPC, was synthesized and characterized by ^{1}H-NMR, FT-IR, and GC-MS. It exhibits high selectivity and sensitivity toward Zn^{2+} ions in a DMF environment over other competitive metal ions. Its detection limit for Zn^{2+} ions is 7.78×10^{-8} M. The sensing mechanism was most likely based on a photo-induced charge transfer effect of complexation between the TPC and Zn^{2+} ions. The 1:1 stoichiometry of the complex formation between Zn^{2+} and TPC was determined by using a Job plot. The DFT and TD-DFT calculations by the cam-B3LYP/6-31G (d,p) method were also carried out to find the optimization structure of TPC. The calculated absorption and emission spectra of the TPC ligand in DMF solvation are 347 and 422 nm, respectively. Both spectra show the main configuration assignments, with HOMOs to LUMOs, indicating the electronic distribution transferring from the thiophene moiety (donor group) to the cyanoacrylic moiety (acceptor group).

Acknowledgments

The authors express their gratitude to the Nanotechnology and Material Analytical Instrument Service Unit (NMIS), School of Integrated Innovative Technology, King Mongkut's Institute of Technology Ladkrabang for instrument support.

References

1 B. L. Vallee and K. H. Falchuk: Physiol. Rev. **73** (1993) 79. https://doi.org/10.1152/physrev.1993.73.1.79
2 J. M. Berg and Y. Shi: Science **271** (1996) 1081. https://doi.org/10.1126/science.271.5252.1081
3 Y. P. Kumar, P. King, and V. S. R. K. Prasad: Chem. Eng. J. **124** (2006) 63. https://doi.org/10.1016/j.cej.2006.07.010
4 M. P. Cuajungco and G.J. Lees: Brain Res. Rev. **23** (1997) 219. https://doi.org/10.1016/S0165-0173(97)00002-7
5 A. I. Bush: Trends Neurosci. **26** (2003) 207. https://doi.org/10.1016/S0166-2236(03)00067-5
6 J. H. Weiss, S. L. Sensi, and J. Y. Koh: Trends Pharmacol. Sci. **21** (2000) 395. https://doi.org/10.1016/S0165-6147(00)01541-8
7 M. P. Cuajungco and G. J. Lees: Neurobiol. Dis. **4** (1997) 137. https://doi.org/10.1006/nbdi.1997.0163
8 U. C. Saha, B. Chattopadhyay, K. Dhara, S. K. Mandal, S. Sarkar, A. R. Khuda-Bukhsh, M. Mukherjee, M. Helliwell, and P. Chattopadhyay: Inorg. Chem. **50** (2011) 1213. https://doi.org/10.1021/ic1015252
9 E. Kimura and S. Aoki: Zinc Biochemistry, Physiology, and Homeostasis, W. Maret, Ed. (Springer, Dordrecht, 2001) pp. 5–18.
10 K. Kikuchi, K. Komatsu, and T. Nagano: Curr. Opin. Chem. Biol. **8** (2004) 182. https://doi.org/10.1016/j.cbpa.2004.02.007
11 S. Mizukami, S. Okada, S. Kimura, and K. Kikuchi: Inorg. Chem. **48** (2009) 7630. https://doi.org/10.1021/ic900247r
12 P. Jiang and Z. Guo: Coord. Chem. Rev. **248** (2004) 205. https://doi.org/10.1016/j.cct.2003.10.013
13 Z. Xu, J. Yoon, and D. R. Spring: Coord. Chem. Rev. **39** (2010) 1996. http://dx.doi.org/10.1039/B916287A
14 B. Valeur and I. Leray: Coord. Chem. Rev. **205** (2000) 3. https://doi.org/10.1016/S0010-8545(00)00246-0
15 S. Aslam, I. Kousar, S. Rani, W. Altaf, S. Bristy and R. Skouta: Molecules **30** (2025) 1450. https://doi.org/10.3390/molecules30071450
16 J. R. Lakowicz: Principles of Fluorescence Spectroscopy (Springer, New York, 2006) 3rd ed.
17 H. G. Loehr and F. Voegtle: Acc. Chem. Res. **18** (1985) 65. https://doi.org/10.1021/ar00111a001
18 J. R. Albani: Principles and Applications of Fluorescence Spectroscopy (Wiley, 2007).
19 B. Valeur and M. N. Berberan-Santos: Molecular Fluorescence: Principles and Applications (Wiley-VCH, Weinheim, 2012) 2nd ed.

20 L. Deng, W. Wu, H. Guo, J. Zhao, S. Ji, X. Zhang, X. Yuan, and C. Zhang: J. Org. Chem. **76** (2011) 9294. https://doi.org/10.1021/jo201487m
21 R. Mishra, K. K. Jha, S. Kumar, and I. Tomer: Der Pharma Chem. **3** (2011) 38. https://www.derpharmachemica.com/pharma-chemica/synthesis-properties-and-biological-activity-of-thiophene-a-review.pdf?utm_source=chatgpt.com
22 A. Chaudhary, K. K. Jha, and S. Kumar: J. Adv. Sci. Res. **3** (2012) 3. https://sciensage.info/index.php/JASR/article/view/106
23 A. Dreiem and F. Fonnum: NeuroToxicology **25** (2004) 959. https://doi.org/10.1016/j.neuro.2004.04.001
24 S. Jana, S. Dalapati, M.A. Alam, and N. Guchhait: J. Photochem. Photobiol., A **238** (2012) 7. https://doi.org/10.1016/j.jphotochem.2012.04.002
25 W.-C. Lin, C.-Y. Wu, Z.-H. Liu, C.-Y. Lin, and Y.-P. Yen: Talanta **81** (2010) 1209. https://doi.org/10.1016/j.talanta.2010.02.012
26 Y. Chen, Z.-H. Sun, B.-E. Song, and Y. Liu: Org. Biomol. Chem. **9** (2011) 5530. http://dx.doi.org/10.1039/C1OB05221G
27 H. Wang, J. Lin, W. Huang, and W. Wei: Sens. Actuators, B **150** (2010) 798. https://doi.org/10.1016/j.snb.2010.07.025
28 S.-K. Chung, Y.-R. Tseng, C.-Y. Chen, and S.-S. Sun: Inorg. Chem. **50** (2011) 2711. https://doi.org/10.1021/ic101908p
29 S. Pandey, A. Azam, S. Pandey, and H. M. Chawla: Org. Biomol. Chem. **7** (2009) 269. http://dx.doi.org/10.1039/B815379E
30 P. Job: Ann. Chim. **9** (1928) 113.
31 M. J. Frisch, G. W. Trucks, H. B. Schlegel, G. E. Scuseria, M. A. Robb, J. R. Cheeseman, G. Scalmani, V. Barone, G. A. Petersson, H. Nakatsuji, X. Li, M. Caricato, A. Marenich, J. Bloino, B. G. Janesko, R. Gomperts, B. Mennucci, H. P. Hratchian, J. V. Ortiz, A. F. Izmaylov, J. L. Sonnenberg, D. Williams-Young, F. Ding, F. Lipparini, F. Egidi, J. Goings, B. Peng, A. Petrone, T. Henderson, D. Ranasinghe, V. G. Zakrzewski, J. Gao, N. Rega, G. Zheng, W. Liang, M. Hada, M. Ehara, K. Toyota, R. Fukuda, J. Hasegawa, M. Ishida, T. Nakajima, Y. Honda, O. Kitao, H. Nakai, T. Vreven, K. Throssell, J. A. Montgomery Jr., J. E. Peralta, F. Ogliaro, M. Bearpark, J. J. Heyd, E. Brothers, K. N. Kudin, V. N. Staroverov, T. Keith, R. Kobayashi, J. Normand, K. Raghavachari, A. Rendell, J. C. Burant, S. S. Iyengar, J. Tomasi, M. Cossi, J. M. Millam, M. Klene, C. Adamo, R. Cammi, J. W. Ochterski, R. L. Martin, K. Morokuma, O. Farkas, J. B. Foresman, and D. J. Fox: Gaussian 09, Revision A.02 (Gaussian, Inc., Wallingford CT, 2016).
32 X.-Q. Zhang, Z.-G. Chi, B.-J. Xu, H.-Y. Li, W. Zhou, X.-F. Li, Y. Zhang, S.-W. Liu, and J.-R. Xu: J. Fluoresc. **21** (2011) 133. https://doi.org/10.1007/s10895-010-0697-y
33 J. Lu, L. Zhang, L. Liu, G. Liu, D. Jia, D. Wu, and G. Xu: Spectrochim. Acta, Part A **71** (2008) 1036. https://doi.org/10.1016/j.saa.2008.02.048
34 M. Formica, V. Fusi, L. Giorgi, and M. Micheloni: Coord. Chem. Rev. **256** (2012) 170. https://doi.org/10.1016/j.ccr.2011.09.010
35 A. K. Mahapatra, S. K. Manna, C. D. Mukhopadhyay, and D. Mandal: Sens. Actuators, B **200** (2014) 123. https://doi.org/10.1016/j.snb.2014.04.034
36 L. Li, Y.-Q. Dang, H.-W. Li, B. Wang, and Y. Wu: Tetrahedron Lett. **51** (2010) 618. https://doi.org/10.1016/j.tetlet.2009.11.070
37 B. Kupcewicz, A. Kaczmarek-Kedziera, K. Lux, P. Mayer, and E. Budzisz: Polyhedron **55** (2013) 259. https://doi.org/10.1016/j.poly.2013.03.035
38 B.-M. Kukovec, I. Kodrin, Z. Mihalić, and Z. Popović: Inorg. Chim. Acta **378** (2011) 154. https://doi.org/10.1016/j.ica.2011.08.050
39 D.-d. Qin, Z.-y. Yang, and G.-f. Qi: Spectrochim. Acta, Part A **74** (2009) 415. https://doi.org/10.1016/j.saa.2009.06.037
40 P. Thanakit, P. Chittratan, S. Pratontep, and D. S.-T. Phromyothin: Integr. Ferroelectr. **155** (2014) 119. https://doi.org/10.1080/10584587.2014.905372